Surface-wave-enabled darkfield aperture for background suppression during weak signal detection

Guoan Zheng[1], Xiquan Cui, and Changhuei Yang

Department of Electrical Engineering, California Institute of Technology, Pasadena, CA 91125

Edited by F. Javier García de Abajo, University of the Basque Country, Spain, and accepted by the Editorial Board March 17, 2010 (received for review November 2, 2009)

Sensitive optical signal detection can often be confounded by the presence of a significant background, and, as such, predetection background suppression is substantively important for weak signal detection. In this paper, we present a novel optical structure design, termed surface-wave-enabled darkfield aperture (SWEDA), which can be directly incorporated onto optical sensors to accomplish predetection background suppression. This SWEDA structure consists of a central hole and a set of groove pattern that channels incident light to the central hole via surface plasmon wave and surface-scattered wave coupling. We show that the surface wave component can mutually cancel the direct transmission component, resulting in near-zero net transmission under uniform normal incidence illumination. Here, we report the implementation of two SWEDA structures. The first structure, circular-groove-based SWEDA, is able to provide polarization-independent suppression of uniform illumination with a suppression factor of 1230. The second structure, linear-groove-based SWEDA, is able to provide a suppression factor of 5080 for transverse-magnetic wave and can serve as a highly compact (5.5 micrometer length) polarization sensor (the measured transmission ratio of two orthogonal polarizations is 6100). Because the exact destructive interference balance is highly delicate and can be easily disrupted by the nonuniformity of the localized light field or light field deviation from normal incidence, the SWEDA can therefore be used to suppress a bright background and allow for sensitive darkfield sensing and imaging (observed image contrast enhancement of 27 dB for the first SWEDA).

surface plasmon | nanophotonics | cell imaging | biological and chemical sensing

The ability of a sensor to observe a weak optical signal in the presence of a strong background can be significantly limited even if the sensor is fully capable of measuring the same weak signal in the absence of background (1, 2). There are several factors that can contribute to this degradation in sensitivity, and their relative significance is dependent on the measurement scenarios involved.

The case of stars in the sky provides a good illustration of some of these limitations. A bright star that is quite visible at night may disappear from our sight during the day. This disappearing act is attributable to two major factors. First, the bright daytime background can introduce a proportionate noise term that the brightness of the star must exceed to be observable. Second, our eyes naturally adjust their dynamic range to accommodate the bright daytime background. As the bit depths of most measurement systems (including our eyes) are finite, we necessarily view the sky with a coarser brightness scale during the day. If the incremental brightness of the star versus the background is smaller than this gradation scale, the star is simply indistinguishable from its background.

The approach of adding bit depth can address part of the problem; however, it is an "engineering" solution that comes at a price of more sophisticated electronics and greater data volume. Moreover, it does not eliminate the proportionate noise term from the background. Interference arrangements can potentially be employed to destructively interfere and cancel the background (for situations where the light sources involved are coherent). However, such schemes are understandably elaborate and nontrivial to employ. A sensor that can intrinsically cancel a strong background prior to signal detection would be a simpler solution with broad applicability.

In this paper, we report a unique sensor structure that accomplishes this type of darkfield sensing for coherent light field in a robust, compact, and simple format. This structure, termed surface-wave-enabled darkfield aperture (SWEDA), generates a surface-wave-enabled component that interferes destructively with the direct light transmission component. As such, a SWEDA-bearing sensor will detect no signal when illuminated by a uniform light field at normal incidence. A SWEDA-bearing sensor is insensitive to the background normal incidence light field but is, instead, highly sensitive to weak localized light field variations or light fields at nonzero incident angles that disrupt the exquisitely balanced interference condition.

We will next describe the operating principle of the proposed structure. Then, we will report on our simulations and experimental implementation of a polarization-independent SWEDA, which utilizes a circular groove pattern for surface wave coupling. We next extend the SWEDA concept to a polarization-sensitive case by using a linear groove pattern for surface wave coupling. Finally, we report on our experimental demonstration of the ability of the circular-groove-based SWEDA to detect weak signals in the presence of a strong background; we also present a proof of concept that, among other applications, shows that sensors based on such structures can be used to implement a new class of darkfield microscopes.

Results

SWEDA Concept. The light interaction between the subwavelength features on a metal-dielectric interface has been a subject of intensive study in recent years (3–12). It has been shown that appropriately patterned rings of metal corrugation around a hole can significantly change the total amount of light transmission through the aperture (3, 5, 7, 8, 10, 11). One primary component involved in such a light interaction between the central hole and the metal corrugation is the surface plasmon (SP) wave, the electromagnetic surface wave existing at the interface between a dielectric and a noble metal (13). Recently, some theoretical and

Author contributions: G.Z. and C.Y. designed research; G.Z. performed research; G.Z. analyzed data; and G.Z., X.C., and C.Y. wrote the paper.

The authors declare no conflict of interest.

This article is a PNAS Direct Submission. F.D. is a guest editor invited by the Editorial Board.

Freely available online through the PNAS open access option.

[1]To whom correspondence should be addressed. E-mail: gazheng@caltech.edu.

This article contains supporting information online at www.pnas.org/lookup/suppl/doi:10.1073/pnas.0912563107/-/DCSupplemental.

experimental results (5–9, 12) also show that the SP wave is not the only component involved in the light interaction of subwavelength features on the metal-dielectric interface. A surface scattered component also plays a role at the short range interaction. Therefore, the mediated-transmission behavior of this corrugation-based aperture can be intuitively explained as follows. When light falls on a patterned groove structure on the metal, it couples into the surface wave, including the SP wave and the surface scattered wave. By choosing the groove periodicity such that the surface wave launched at each groove adds up in phase, we can generate a strong propagative surface wave that is directed toward the hole. The surface wave can then be converted back to a propagating optical wave at the central hole. In essence, the groove structure serves as an antenna for light collection and uses the surface wave to transport the collected optical power to the hole. Using this approach, researchers have reported both light transmission enhancement and suppression (3, 5, 7, 10, 14).

Our SWEDA design differs from previous surface-wave-modulated aperture design by exactly balancing the direct transmission component of the central hole and the surface wave component induced from the grooves (for clarity, we refer to the center opening as the central hole and the entire structure as the aperture). This creates a situation where the two transmission components can interact significantly—thus providing an additional means for light manipulation. To be specific, we precisely control the amplitude of the surface wave by changing the periodicity and depth of the groove structure. Through judicious choice of the groove structure and the central hole size, we can arrive at a situation where the surface wave component is equal in strength to the direct transmission component. Furthermore, we can adjust the phase lag between the surface wave and the direct transmission component by choosing the gap between the innermost groove and hole appropriately. If we adjust this phase lag such that the optical wave generated by the surface wave component is 180° out of phase with the direct transmission component, the two components will destructively interfere and result in little or no light transmits through the hole in the presence of uniform normal-incidence illumination. Because this destructive interference condition critically depends on an exact balance of the two mentioned components, a small change in spatial distribution of the input light field intensity or phase will disrupt the destructive interference condition and permit significant light transmission through the hole.

In the context of high-sensitivity optical signal detection, the advantage of SWEDA can be easily appreciated. The structure can effectively suppress a uniform normal-incidence background from reaching the underlying sensor and instead only permit highly localized light field variations or light fields at nonzero incidence angles to pass through and be detected. As such, the underlying sensor no longer needs to contend with a high background and its associated noise fluctuation terms. The bit depth can also be optimized and devoted to the detection of the weaker light field variations. Used in an appropriate manner, such devices can potentially allow for greater signal detection sensitivity in "weak signal buried in high background" scenarios. This method also enables a unique way to build darkfield microscopes on the sensor level that does not rely on elaborate bulk optical arrangements.

SWEDA with Circular Groove Pattern. The first type of SWEDA is shown in Fig. 1*A*. It adopts a circular pattern for the groove design. We refer to this structure as the circular-groove-based SWEDA. Due to its circular symmetry nature, this type of SWEDA provides a polarization-independent behavior for signal detection and imaging. We began the implementation of such a SWEDA by using a commercial software—CST Microwave Studio to perform a set of simulations to understand the interplay between our design parameter choices and system characteristics. The simulations were performed at a nominal wavelength of 738 nm. The permittivity of gold at this wavelength is $-19.95 + 1.48i$ (15). There are primarily 4 specific parameters that impact the performance of the SWEDA: (*i*) Groove periodicity and groove depth. The groove periodicity (defined here as the *p*-parameter in Fig. 1*A*) and groove depth can be adjusted to control the magnitude of the surface wave coupled into the structure. Note that the exact match of the groove periodicity to the wavelength of the surface wave is not necessarily desired, as this may induce an overly strong surface wave component. (*ii*) The number of grooves. The strength of the coupled surface wave increases as a function of groove numbers. On the other hand, we desire a low number of grooves for overall SWEDA structure compactness considerations. (*iii*) Central hole size. This affects the strength of the direct transmission component. We would additionally aim to restrict the aperture size such that the light transmission is not multimoded. Multimode light transmission significantly complicates the destructive interference balancing act as we would need to achieve destructive interference between the surface wave component and the direct transmission component for all modes involved. (*iv*) The distance between the innermost groove and the rim of the central hole (defined here as the *s*-parameter in Fig. 1*A*) determines the phase difference between the surface-wave-induced and the direct-transmission components. To accomplish exact cancellation of the two components, we require this phase difference to be 180°. Other parameters such as the groove profile can also be used to tune the surface wave component; however, from the fabrication point of view, the profile of the groove is not as easy to control as the 4 parameters we mentioned.

The simulation program allowed us to map out the interplay of these parameters and the overall SWEDA system characteristics. We define the darkfield suppression factor as the ratio of the total power transmission through a simple hole (without grooves) to the total power through a SWEDA. For good darkfield performance, we desire this ratio to be as high as possible. We were able to arrive at a design parameter set (Fig. 1*A*) that provides a suppression factor of 6640 by the simulation program. The simulated electric field distributions for this particular SWEDA design (Fig. 1*A*) and that of a corresponding simple hole (Fig. 1*B*) are shown here. We can see that the SWEDA structure should indeed be able to suppress light transmission through the central hole significantly. We next simulated the translation of a cylindrical dielectric object (radius 300 nm, thickness 200 nm, displacement height 300 nm, permittivity 2.25) across the top of the SWEDA structure (Fig. 1 *C*–*F*). We can see that the SWEDA began to transmit light significantly when the object's presence directly above the central hole significantly perturbed the direct transmission component and, consequently, disrupted the delicately balanced destructive interference condition. We further observed that the presence of the object above the groove structures did perturb the SWEDA to a certain extent as well. However, the impact was much less significant (Fig. 1*F*); this can be well appreciated by noting that the generation of surface wave occurred over the entire area associated with the ring grooves and localized changes of the light field over the area had a diminished impact on the overall surface wave component. As a whole, this simulation indicates that the SWEDA is maximally sensitive to light field heterogeneity directly above the central hole.

We next fabricated a number of SWEDA structure based on the parameters suggested by our simulation results. Fig. 2*A* shows the SEM image of a typical SWEDA that we have created by focus ion beam (FIB) milling (see *Methods* for more details). We fabricated a set of 13 SWEDAs with different spacing "*s*" ranging from 540 nm to 1020 nm. A single hole without the groove structure was also fabricated to serve as a control. To characterize the optical property of the SWEDA, we used a tunable wavelength laser (Spectra–Physics Tsunami continuous wave Ti:

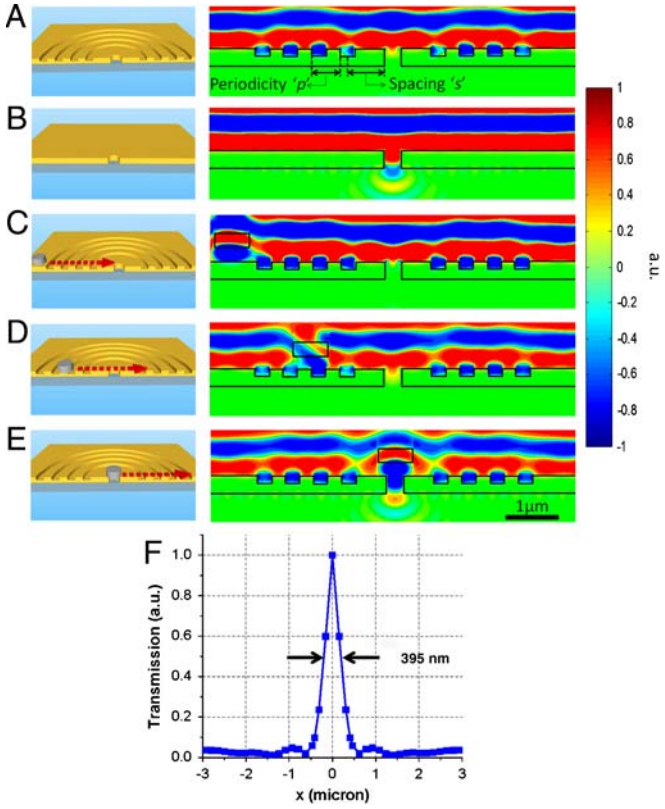

Fig. 1. Simulations of the circular-groove-based SWEDA. Displayed is the real part of the electric-field at $\lambda = 738$ nm (equivalent to the time-domain fields at the instant of time when the source phase is zero). (*A*) The optimized SWEDA structure, where $s = 774.3$ nm, $p = 560$ nm, thickness of gold = 340 nm, diameter of hole = 300 nm, and groove depth = 140 nm and refraction index of the dielectric substrate = 1.5. The simulation predicts that the darkfield suppression factor of this structure equals 6640. (*B*) Simulation for the simple hole. (*C–E*) Simulations of a cylindrical scatterer (radius 300 nm, thickness 200 nm, displacement height 300 nm, permittivity 2.25) transiting across the SWEDA. (*F*) The transmission signal curve from the SWEDA as the cylindrical scatterer (the same as *C–E*) moves across it. The full width at half maximum was determined to be 395 nm.

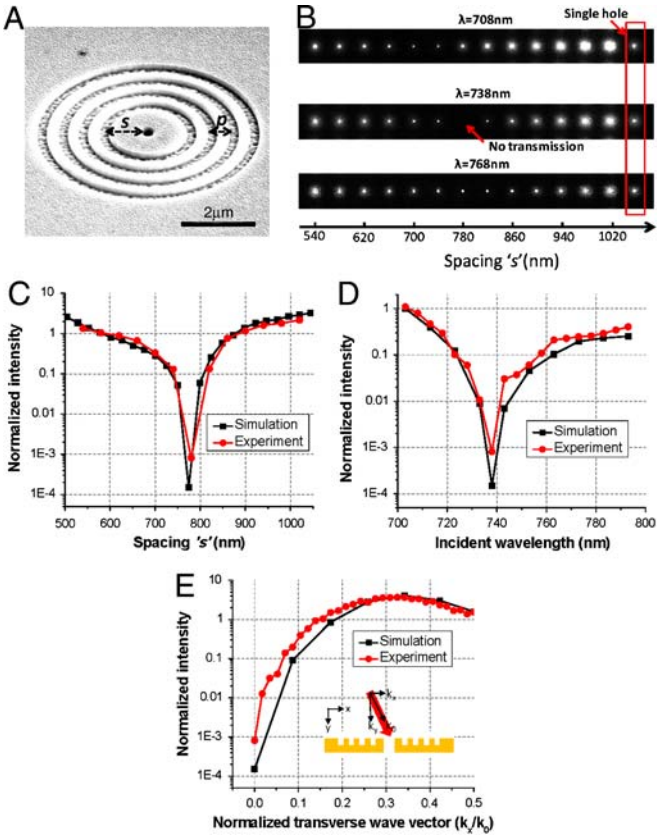

Fig. 2. Experimental characterization of the circular-groove-based SWEDA. (*A*) The SEM image of a typical fabricated SWEDA. (*B*) The optical transmission images of the 13 SWEDAs and the reference single-hole under normal-incidence illumination for three different wavelengths. (*C*) The measured optical transmission signals from SWEDAs with different *s* ranging from 540 to 1020 nm (left to right). The signals from the SWEDA were normalized by single hole (signal from the single hole at normal incidence was set to unity). The simulated intensity is also shown for comparison. (*D*) The normalized optical transmission signals of SWEDA ($s = 780$ nm) with different incident wavelengths. (*E*) The normalized optical transmission signals of SWEDA with different normalized transverses wave vector (see *Methods* for more details).

Sapphire) as the illumination source. The transmissions through the apertures were collected by an inverted microscope with a 20X objective lens.

Fig. 2*B* shows the optical transmission images of the 13 SWEDAs and the reference single hole at normal incidence for three different wavelengths. We can see that the spacing parameter *s* does indeed have a significant impact on the transmission of the SWEDA structures. The transmission intensity measured for these SWEDA structures are plotted in Fig. 2*C* (wavelength of 738 nm); we used the unadorned simple hole for normalization. The simulation prediction for each of the structures is also plotted for comparison. From the plots, the implemented SWEDA structure with *s*-parameter of 780 nm exhibited the desired near-zero transmission characteristics. The optimized SWEDA's structure parameters were a close match with our simulation predictions—the *s* parameter differed by 6 nm (<0.8%). The measured suppression factor for the optimized SWEDA was 1230. In other words, this SWEDA transmitted 1230 times less light than an unadorned simple hole of size equal to that of the central SWEDA hole.

We next measured the spectral response of the optimized SWEDA over a spectral range of 700 nm to 790 nm. Because SWEDA's operation depends on the exact amplitude balance and opposing phase relationship of the surface-wave-enabled transmission component and the direct transmission component, we can expect that the darkfield property of SWEDA to be optimized for one single wavelength. Fig. 2*D* shows the experimentally measured and simulation-predicted spectral transmission of the SWEDA. As expected, there is a single minimum over the range of interest and the transmission increased monotonically away from this point. It is also worth noting that the suppression factor actually remained fairly high (>50) for a bandwidth of approximately 10 nm.

For a given incident light field, we can decompose it into different plane wave component with respect to the transverses wave vector (16). In Fig. 2*E*, we measure the transmission of the SWEDA as a function of the normalized transverses wave vector (k_x/k_0). Fig. 2*E* represents the system transfer function of the SWEDA: SWEDA rejects the normal incident plane wave component and transmits other components with efficiency as dictated by this transfer function.

The good agreement between the experimental and simulated spacing, wavelength and transverses wave vector trends, as evident in Fig. 2 *C*, *D*, and *E*, is a proof of the SWEDA working principle. The discrepancy in darkfield suppression factor is attributable to fabrication imperfections associated with the FIB milling process. We tend to end up with rounded structure edges experimentally. Another contribution might be the variation in groove depth due to the intrinsic roughness of the groove bottom (metals mill nonuniformly as a function of grain orientation due

to channeling). If exact matches of experiments and simulation are desired in specific applications, such imperfections may be mitigated by employing a sacrificial layer, as described in ref. 17, during fabrication to help preserve the sharpness of edges.

SWEDA with Linear Groove Pattern. The second type of SWEDA is shown in Fig. 3 *A* and *B*. It adopts a linear pattern for the groove design (refer as the linear-groove-based SWEDA), and as such, it is highly sensitive to the polarization state of the incident light. As shown in Fig. 3*A*, incoming transverse-magnetic (TM) polarized light (where the electric field is perpendicular to the groove structure) can be collected and converted into a surface wave by the periodic grooves and then be recoupled into propagating light through the central hole. On the other hand, the TE (with magnetic field perpendicular to the groove structure) coupling efficiency of the SP wave, a major component of the total surface wave, is much smaller than the TM case (13), and thus, the absence of interference with the SP wave permits significant TE polarized light transmission through the hole in Fig. 3*B*. Fig. 3 *C* and *D* show the simulations of this SWEDA at a nominal wavelength of 750 nm [the permittivity of gold at this wavelength is $-20.96 + 1.55i$ (15)]. We were able to arrive at a set of design parameters that provide a darkfield suppression factor of 35400 for TM wave in our simulations. The simulated magnetic field distributions for this particular design are shown in Fig. 3*C*. In Fig. 3*D*, we also show the electric field distributions for the TE wave, from which we can see that the structure does transmit TE wave significantly. The difference between the TM and TE cases also verifies the surface-wave-enabled mechanism of the linear-groove-based SWEDA, because the SP wave can only be induced efficiently for TM polarization (13). We also note that, from the simulations shown in Fig. 3 *C* and *D*, the linear-groove-based SWEDA provides a polarization extinction ratio of 42500 for the two orthogonal polarization states.

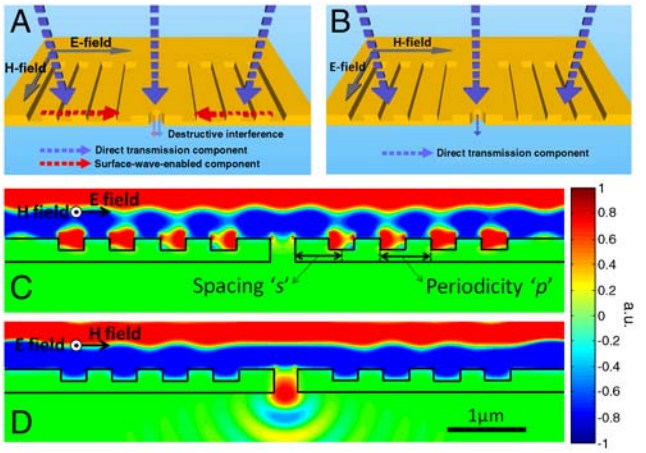

Fig. 3. Working principle and simulation of the linear-groove-based SWEDA. (*A*) The TM incident light is coupled into surface wave by the linear groove pattern. The destructive interference between the surface-wave-enabled component and the direct transmission component results in zero transmission. (*B*) The TE incident light cannot be coupled into SP waves (a primary component of the total surface wave), and transmission is induced in the absence of destructive interference. (*C*) Simulation of the TM case. Displayed is the real part of the electric field at $\lambda = 750$ nm. The parameters of the optimized SWEDA are: $s = 658$ nm, $p = 660$ nm, thickness of gold $=$ 340 nm, diameter of hole $= 300$ nm, groove depth $= 140$ nm, and refractive index of the dielectric substrate $= 1.5$. The simulation predicts a TM darkfield suppression factor of this structure versus a simple hole is 35400. (*D*) Simulation of the TE case. Displayed is the real part of the magnetic field at $\lambda = 750$ nm. The simulation predicts the polarization extinction ratio of the two orthogonal polarization states is 42500.

We next fabricated a number of linear-groove-based SWEDAs with linear-groove patterns. Fig. 4*A* shows the SEM image of a typical linear-groove-based SWEDA that we have created by FIB milling. We fabricated a set of 9 linear-groove-based SWEDAs with different spacing s ranging from 455 nm to 775 nm. The optical transmission signals of linear-groove-based SWEDAs are normalized and plotted as a function of spacing s and wavelength λ in Fig. S1. The measured darkfield suppression factor for the optimized linear-groove-based SWEDA was 5080. In other words, this structure transmitted 5080 times less TM light than an unadorned simple hole of size equal to that of the central SWEDA opening. In Fig. 4*B*, a light field is incident on the SWEDA with a polarization angle θ—this geometry is used for our subsequent measurements. The optical images with different polarization angles are shown in Fig. 4*C*, and the normalized signals of SWEDAs are plotted in Fig. 4*D*. The measured polarization extinction ratio is 6100, meaning that the amount of TE light transmission through the linear-groove-based SWEDA is 6100 times higher than the TM case. Such a high extinction ratio positively indicates that the linear-groove-based SWEDA can serve as a highly compact and highly efficient polarization sensor.

Demonstration of the Circular-Groove-Based SWEDA's Ability to Boost Detection Sensitivity. Due to the polarization-independent nature of the circular-groove-based SWEDA, it can be used to suppress a bright normal-incidence background regardless of the incident light field's polarization state. The ability of such a SWEDA to improve small signal detection is illustrated in the following experiment. We prepared a sample comprised of an indium tin oxide (ITO)-coated glass slide that was marked with shallow pits of radius of 175 nm and 250 nm via the FIB (Fig. 5*A* and *B*). Next, we transmitted a uniform light field of intensity about 0.2 W/cm^2 from a 738 nm laser through the sample. We then used a 1 : 1 relay microscope to project a virtual image of the pits onto our optimized circular-groove-based SWEDA (see *Methods* for more details). We next raster-scanned the sample and measured the light transmission through the SWEDA at each point of the scan. We then generated an image of the sample from the collected data. As is evident in Fig. 5*C* and *D*, SWEDA allowed us to identify the presence of the two pits with little difficulty. We next acquired

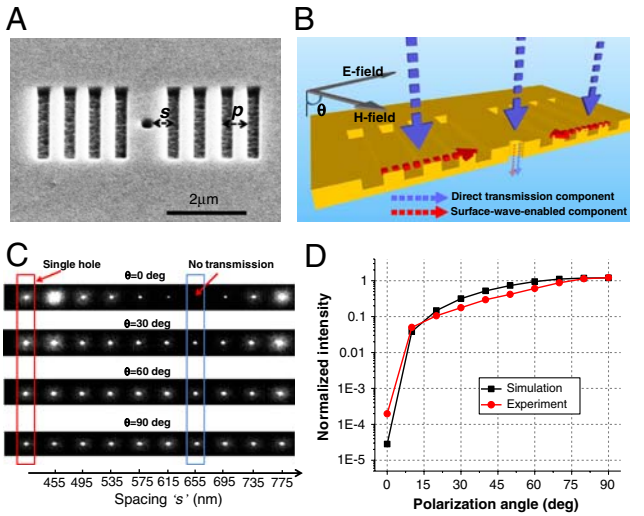

Fig. 4. Experimental characterization of the linear-groove-based SWEDA. (*A*) The SEM image of a typical fabricated SWEDA. (*B*) The light is incident on the SWEDA with a polarization angle θ. (*C*) The optical transmission images of the SWEDAs for different polarization angles at $\lambda = 750$ nm. (*D*) The normalized optical transmission signals of SWEDA are plotted as a function of polarization angle. The measured polarization extinction ratio for TE and TM incidence is 6100.

images of the same pits (Fig. 5*E* and *F*) with a simple camera (based on the same sensor chip). It is difficult to identify the presence of the two pits in this case. The total light fluence incident on the sample for both the SWEDA and camera image acquisitions was kept the same to allow for direct result comparisons.

Fig. 5*G* shows plots of signal traces across the images. The SWEDA-acquired data were normalized on the same scale. The camera image data were normalized versus the average background signal. The backgrounds associated with the SWEDA-acquired data were low and the contributive signals from the pits were well discernible. In fact, the contributive signals were sufficiently well-resolved that we can use them to quantify their relative strengths for the two pits. In comparison, the high backgrounds in the camera images combined with the associated noise masked the scattering contributions from the pits. The measured contrast improvement was 25 dB for the 175 nm pit and 27 dB for the 250 nm pit.

As pointed out in our introduction, circular-groove-based SWEDA can potentially be employed to perform darkfield microscopy imaging at the sensor level. The principle involved is substantially different from that of a conventional darkfield microscope. Whereas a conventional system depends on oblique illumination and a relatively small objective angle of collection to screen out the uniform background via a fairly sophisticated bulk optical arrangement, the ability of circular-groove-based SWEDA to screen out uniform background presents a more direct approach. To demonstrate that such a system can indeed be implemented, we employed our optimized circular-groove-based SWEDA in the same experimental scheme to scan slides of starfish embryos in different developmental stages. The illumination intensity was 0.2 W/cm^2. Fig. 5*H* and *J* show the results. Similar images of the specimens taken with a standard microscope are shown in Fig. 5*I* and *K* for comparison. We can see that the SWEDA generated image has a dark background, as is consistent with a darkfield microscope image. We can also see that the edge and interior of the starfish embryo appeared brighter in the SWEDA image and darker in the control image. This is again consistent with our expectations of a darkfield image as sample locations with substantial scattering should appear brighter in a darkfield image and darker in a simple transmission image. We would like to emphasize that this is a proof of concept experiment. A feasible darkfield microscope can be implemented by employing a laser as the light source in a standard microscope and using a sensor chip patterned with a grid of tightly spaced circular-groove-based SWEDA as the microscope camera.

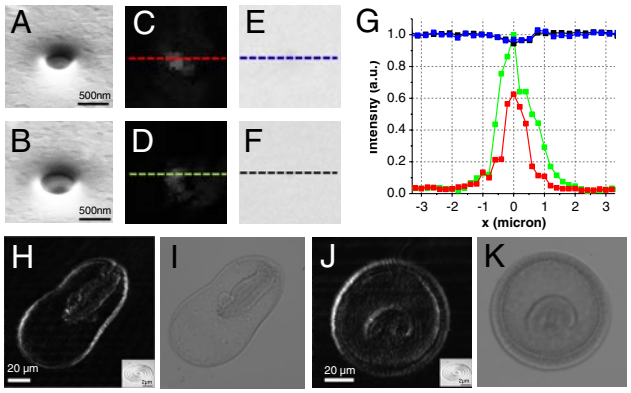

Fig. 5. The sensitivity enhancement demonstration for the circular-groove-based SWEDA. (*A* and *B*) The SEM images of the 175 and 250 nm pits on the ITO-coated glass. (*C* and *D*) The SWEDA-based raster-scanned images of the samples (*A*) and (*B*). (*E* and *F*) Microscope images of the samples (*A*) and (*B*) under the same illumination condition as the SWEDA collected images using a conventional camera with the same complementary metal oxide semiconductor (CMOS) chip. (*G*) Center line traces of the images in (*C*–*F*). Please see (*C*–*F*) for color reference guide. The observed image contrast (signal/background) enhancement is approximately 25 dB for the 175 nm pit and approximately 27 dB for the 250 nm pit. (*H* and *J*) The SWEDA-based raster-scanned images of the starfish embryos. (*I* and *K*) Conventional bright field microscope images.

Discussion

As our experimental findings indicate, SWEDA is a robust, structurally simple and highly compact approach to accomplish optical background suppression and/or polarized light field suppression. It is also worth noting that, in principle, there is no theoretical limit to how close the SWEDA darkfield suppression factor can approach infinity; the practical limit is only set by the fabrication tolerance and the net transmission through the opaque metal layer.

There are a few limitations associated with the SWEDA structure that are worth discussing presently. First, the structure is optimized for single wavelength operations. This limitation can be overcome by using more complicated SWEDA-type structures involving multibeam interference that can operate over a broad range of wavelengths. Second, the amount of light transmitted is largely limited by the size of the central hole. We believe that this issue can be potentially addressed by replacing the central opening of SWEDA with multiple C-shape apertures (18) to increase light collection efficiency. Third, this structure works well at only blocking uniform light field at normal incidence. Fortunately, the general SWEDA concept can be extended with asymmetric structure designs to screen out light at other incidence angles.

SWEDA technology can potentially be used in a range of different applications. The linear-groove-based SWEDA demonstrated in the present work is a highly compact and highly sensitive polarization sensor. Because the polarization state of light will change during the interaction with chiral materials, this SWEDA design may also find some applications in on-chip detection of some chiral materials such as sugar, proteins, and DNA (19, 20). The ability to fully suppress a coherent background as exhibited by the circular-groove-based SWEDA can be useful for small signal detections in metrology applications. It is especially applicable in detection scenarios where the overall background intensities fluctuate with time. As our background subtraction occurs at the individual pixel level, SWEDA technology removes the need for balanced detection schemes. The predetection background subtraction, which is a light cancellation process, is also intrinsically more sensitive than postdetection cancellation schemes that are susceptible to intrinsic detection statistical variations. The inclusion of chemical reagents in the central hole can also turn such a SWEDA structure into a high-sensitivity sensor that can react to small refractive index changes of the reagents.

From a practical implementation viewpoint, SWEDA structures can be fabricated directly on top of CCD or CMOS sensor pixels. The small size and planar design of SWEDA make such implementation particularly suited for foundry fabrication. Sensor chips with broad-bandwidth SWEDA can then be used in place of the standard camera sensor to accomplish sensor level darkfield imaging. Such systems, in combination with a coherent light source, can transform a standard microscope into a simpler and cheaper darkfield microscope than current darkfield microscopes. Such systems can also enable edge-detection imaging in machine vision applications if the illumination source employed is coherent. A SWEDA array can also replace the hole array in the optofluidic microscope (OFM) (21)—a low-cost, lensless and high resolution microscopy approach, to accomplish darkfield microscopy imaging on a chip. The use of SWEDA in this case is especially appropriate as both the OFM and SWEDA implementation are well suited for semiconductor mass fabrication. In fact, it is difficult to envision a more compact and cost-effective approach for incorporating darkfield ability in an OFM system.

Finally, we would like to note that the general concept of exact balancing the surface-wave-enabled component and direct light transmission component in a destructive interference manner is a unique idea that can inspire other surface-wave structures with novel properties. Effectively, such structures are tiny interferometers (approximately 6 micrometers or less) that can be fabricated on a single metal substrate and that have excellent stability (our SWEDA structures exhibited no significant performance drift over the entire duration of our experiments). Because the structure is planar, it can be mass produced in a semiconductor foundry. The proposed structure can also be redesigned for operation at longer wavelengths. As an example of other potential applications, we believe that the concept of SWEDA can be applied to optical isolation in a ultracompact format, polarization control in semiconductor lasers (22), wavefront detection, extending depth of field of the type II aperture-based imaging device (23), and perspective imaging (24) by customizing the optical transfer function on the pixel level.

Methods

Simulation. The simulations were performed in 3 dimensions. The calculation domain was $12\lambda \times 12\lambda \times 3\lambda$ and contained approximately 12 million meshes. The transmission of the SWEDA and single hole were calculated by integrating the Poynting vector over a $6\lambda \times 6\lambda$ region (0.85λ beneath the aperture). For all simulations, we applied a perfect match layer at the outer boundaries.

Sample Preparation. We started with a 2 nm thick titanium layer (adhesion layer) and 340 nm thick gold layer that were coated on a 1 mm thick glass substrate by an e-beam evaporator (Temescal BJD-1800). A focused ion beam (FEI Nova200 dual-beam system using Ga^+ ions with a 5 nm nominal beam diameter) was employed to perform milling. A low ion beam current was used (30 pA, 30 keV) in the milling process to accomplish the requisite fine structure.

Optical Setup. For Fig. 2*E*, the transmission of the SWEDA is collected by a 20X objective and the whole detection setup is assembled on a motorized rotation stage to measure the spatial response of the aperture with different transverse wave vector of the incident light. The sensitivity enhancement demonstration for the circular-groove-based SWEDA (Fig. 5) was conducted in a laboratory-built 1:1 relay microscope (25). The collection element employed in the relay microscope was a 0.4 numerical aperture Olympus objective. We used the relay microscope to project the virtual image of the sample onto our optimized circular-groove-based SWEDA. We accomplished imaging by raster-scanning the sample. The scanning process was controlled by two motorized actuators (Newport, LTA-HS) and a motion controller (Newport, ESP301). The motion step was 200 nm for Fig. 5 *C* and *D* and 1.5 μm for Fig. 5 *H* and *J*.

ACKNOWLEDGMENTS. We are grateful for the constructive discussions with and the generous help from Professor Axel Scherer (Caltech); Dr. Xin Heng (BioRad); and Dr. Meng Cui, Dr. Emily McDowell, Ms. Yingmin Wang, Dr. Jigang Wu, Mr. Jian Ren, and Mr. Lap Man Lee (Caltech). We appreciate the assistance of Kavli Nanoscience Institute at Caltech. This work is funded by the Wallace Coulter Foundation, the National Science Foundation Career Award BES-0547657, and the National Institutes of Health Grant R21EB008867-01.

1. Narayanaswamy R, Wolfbeis O (2004) *Optical Sensors: Industrial, Environmental and Diagnostic Applications* (Springer, Berlin).
2. Cox GC (2007) *Optical Imaging Techniques in Cell Biology* (Taylor and Francis, Boca Raton, FL).
3. Thio T, et al. (2001) Enhanced light transmission through a single subwavelength aperture. *Opt Lett* 26:1972–1974.
4. Lezec H, et al. (2002) Beaming light from a subwavelength aperture. *Science* 297:820–822.
5. Lezec H, Thio T (2004) Diffracted evanescent wave model for enhanced and suppressed optical transmission through subwavelength hole arrays. *Opt Express* 12:3629–3651.
6. Chen L, et al. (2006) Role of radiation and surface plasmon polaritons in the optical interactions between a nano-slit and a nano-groove on a metal surface. *Opt Express* 14:12629–12636.
7. Gay G, et al. (2006) The optical response of nanostructured surfaces and the composite diffracted evanescent wave model. *Nat Phys* 2:262–267.
8. Lalanne P, Hugonin J (2006) Interaction between optical nano-objects at metallo-dielectric interfaces. *Nat Phys* 2:551–556.
9. Aigouy L, et al. (2007) Near-field analysis of surface waves launched at nanoslit apertures. *Phys Rev Lett* 98:153902.
10. Pacifici D, et al. (2007) All-optical modulation by plasmonic excitation of CdSe quantum dots. *Nat Photonics* 1:402–406.
11. Laux E, et al. (2008) Plasmonic photon sorters for spectral and polarimetric imaging. *Nat Photonics* 2:161–164.
12. Ung B, Sheng Y (2008) Optical surface waves over metallo-dielectric nanostructures: Sommerfeld integrals revisited. *Opt Express* 16:9073–9086.
13. Maier S (2007) *Plasmonics: Fundamentals and Applications* (Springer, Berlin).
14. Pacifici D, et al. (2008) Quantitative determination of optical transmission through subwavelength slit arrays in Ag films: Role of surface wave interference and local coupling between adjacent slits. *Phys Rev B* 77:115411.
15. Palik E, Ghosh G (1985) *Handbook of Optical Constants of Solids* (Academic, New York).
16. Kong J (2005) *Electromagnetic Wave Theory* (EMW Publishing, Cambridge, MA).
17. Leen J, et al. (2008) Improved focused ion beam fabrication of near-field apertures using a silicon nitride membrane. *Opt Lett* 33:2827–2829.
18. Shi X, et al. (2003) Ultrahigh light transmission through a C-shaped nanoaperture. *Opt Letters* 28:1320–1322.
19. Fasman G (1996) *Circular Dichroism and the Conformational Analysis of Biomolecules* (Plenum, New York).
20. Minakawa K, et al. (2009) Microchamber device equipped with complementary metal oxide semiconductor optical polarization analyzer chip for micro total analysis system. *Jpn J Appl Phys* 48:04C192.
21. Cui X, et al. (2008) Lensless high-resolution on-chip optofluidic microscopes for *Caenorhabditis elegans* and cell imaging. *Proc Natl Acad Sci USA* 105:10670–10675.
22. Yu N, et al. (2009) Semiconductor lasers with integrated plasmonic polarizers. *Appl Phys Lett* 94:151101.
23. Heng X, et al. (2006) Characterization of light collection through a subwavelength aperture from a point source. *Opt Express* 14:10410–10425.
24. Levoy M (2006) Light fields and computational imaging. *Computer* 39:46–55.
25. Cui X, et al. (2008) Quantitative differential interference contrast microscopy based on structured-aperture interference. *Appl Phys Lett* 93:091113.